

Pair-density-wave superconductivity and Anderson's theorem in bilayer nickelates

Hanbit Oh^{1,*} and Ya-Hui Zhang¹

¹ *William H. Miller III Department of Physics and Astronomy,
Johns Hopkins University, Baltimore, Maryland, 21218, USA*

(Dated: December 23, 2025)

The recent experimental observations of high temperature superconductivity in bilayer nickelate have attracted lots of attentions. Previous studies have assumed a mirror symmetry \mathcal{M} between the two layers and focused on uniform and clean superconducting states. Here, we show that breaking this mirror symmetry via an applied displacement field can stabilize a pair-density-wave (PDW) superconductor, which is similar to the Fulde–Ferrell–Larkin–Ovchinnikov (FFLO) state, but at zero magnetic field. Based on a mean-field analysis of a model of $d_{x^2-y^2}$ orbital with an effective inter-layer attraction, we demonstrate that the PDW phase is robust over a wide range of displacement field, interlayer hopping strengths, and electron fillings. Finally, we analyze disorder effects on interlayer superconductivity within the first Born approximation. Based on symmetry considerations, we show that pairing is weaken by disorders which break the mirror symmetry, even with unbroken time reversal symmetry. Our results establish bilayer nickelate as a tunable platform for realizing finite-momentum pairing and for exploring generalized disorder effects.

Introduction.— Bilayer nickelates have recently emerged as a promising platform for exploring high- T_c superconductivity, following the report of 80 K superconductivity in bulk $\text{La}_3\text{Ni}_2\text{O}_7$ [1–4]. Motivated by their structural similarity to cuprates—yet possessing a distinct electronic configuration with a multi-orbital nature—extensive theoretical [5–78] and experimental efforts [79–104] have been dedicated to characterizing this system. More recently, superconductivity with $T_c \sim 40$ K has also been realized at ambient pressure in strained thin films [105–108], providing a unique opportunity to probe the system using more accessible measurement techniques, such as angle-resolved photoemission spectroscopy (ARPES) and scanning tunneling microscopy (STM), to elucidate its electronic and magnetic properties. On the theoretical side, a wide range of studies have been carried out, proposing various mechanisms for the observed superconductivity. One plausible scenario is interlayer s_{\pm} -wave pairing in the $d_{x^2-y^2}$ orbital, driven by strong interlayer superexchange coupling originating from the d_{z^2} orbital via Hund's coupling [5–13]. However, most existing studies assume mirror symmetry between the two layers, which guarantees the nesting condition necessary for interlayer pairing. The regime where mirror symmetry is significantly broken remains largely unexplored.

Bilayer structures introduce internal degrees of freedom that, when symmetry constraints are relaxed, can host unconventional states such as the pair-density-wave (PDW) superconductor [109]. A typical realization of a PDW is the Fulde–Ferrell–Larkin–Ovchinnikov (FFLO) state, which relies on Zeeman splitting and explicitly breaks time-reversal symmetry [110, 111]. Identifying alternative mechanisms for time-reversal-symmetric PDW states remains a significant challenge, and the search for candidate materials is ongoing. In this work, we propose that bilayer nickelates provide a promising platform to re-

alize PDW states by breaking mirror symmetry. Specifically, under the strong interlayer pairing scenario, the resulting superconducting state can acquire a finite center-of-mass momentum upon the application of an external electric field. The momentum of the PDW is determined by the Fermi-surface mismatch between the two layers. Using a mean-field analysis of an effective single-orbital model, we demonstrate the existence of a robust PDW

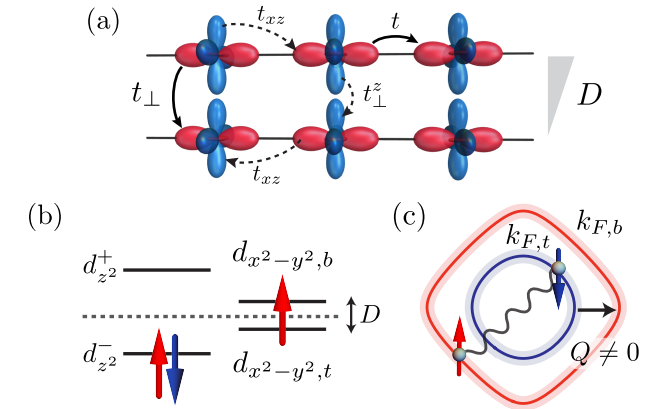


FIG. 1. (a) Schematic illustration of a bilayer nickelate. Each layer forms a square lattice hosting the $d_{x^2-y^2}$ and d_{z^2} orbitals. In the effective one-orbital description of the $d_{x^2-y^2}$ orbital, we only keep inplane hopping t , and effective inter-layer hopping t_{\perp} , generated as a higher-order process in the underlying two-orbital model (dashed arrows). An external displacement field D breaks mirror symmetry between the two layers. (b) The d_{z^2} orbital is nearly half-filled, while the $d_{x^2-y^2}$ orbital is close to quarter filling. The energy levels are shown schematically; in reality, the $d_{x^2-y^2}$ orbital forms a dispersive band with average filling $n = 1 - x$, where x denotes hole doping. (c) Fermi-surface mismatch between the two layers leads to Cooper pairing with finite momentum $\delta k_F = k_{F,t} - k_{F,b}$. For finite t_{\perp} , the two layers are hybridized and Q is generally defined in the band basis.

state over a wide range of the phase space.

In addition, we investigate the interplay between interlayer pairing and disorder in bilayer nickelates. Anderson's theorem [112] states that conventional *s*-wave superconductivity is robust against disorder that preserves time-reversal symmetry. This principle has been generalized to multiband and odd-parity superconductors in several studies [113–116]. Here, we focus on interlayer spin-singlet pairing, where the pairing partners are related by the composite \mathcal{MT} symmetry, combining mirror reflection \mathcal{M} and time-reversal symmetry \mathcal{T} . By employing the superconducting fitness formalism [116, 117] within the conventional Born approximation [118, 119], we show that Anderson's theorem for interlayer pairing can be generalized to the \mathcal{MT} -preserving channel. Moreover, we examine the effects of finite interlayer hopping t_{\perp} . We find that disorder breaking the mirror symmetry \mathcal{M} consistently suppresses interlayer pairing, regardless of the presence of t_{\perp} .

Effective one-orbital model.— The bilayer nickelate can be described by the two-orbital model on square lattice as illustrated in Fig. 1(a) (see SM) [14]. We label $d_{x^2-y^2}$ and d_{z^2} orbitals as d_1 and d_2 . Electron filling is $n = 2 - x$ per site (summed over spin), with $x \approx 0.5$ relevant to experiments, corresponding to orbital fillings $n_1 \approx 0.5$ and $n_2 \approx 1$. The resulting band structure hosts α , β , and γ Fermi pockets, as depicted in Fig. 2(d). It has been shown that α and β pockets exhibit mixed orbital character, while the γ pocket is mainly from the d_2 orbital [14].

We now construct an effective one-orbital model to describe the low-energy physics more efficiently. As argued in Ref. [5, 75], the d_2 orbital is likely close to a Mott insulating state. Therefore, the mobile carriers are dominated by the d_1 orbital. Hence we focus on the α and β Fermi pockets and consider an effective single-orbital model,

$$H_0^{\text{eff}} = \sum_{k,l,\sigma} \xi(\mathbf{k}) n_{k,l,\sigma} + \sum_{k,\sigma} \gamma(\mathbf{k}) c_{k,t,\sigma}^\dagger c_{k,b,\sigma} + \text{H.c.} \quad (1)$$

with

$$\xi(\mathbf{k}) = -2t_x(\cos k_x + \cos k_y) - \mu, \quad (2)$$

and

$$\gamma(\mathbf{k}) = -t_{\perp}(\cos k_x - \cos k_y)^2. \quad (3)$$

Here, $c_{k,l,\sigma} = d_{1,k,l,\sigma}$ denotes the electron operator for the d_1 orbital on layer l . The first term describes in-plane nearest-neighbor hopping within each layer. The second term represents an effective interlayer hopping t_{\perp} , which arises as a higher-order process. Phenomenologically, this interlayer hopping can be understood as a second-order process involving inter-orbital hopping t_{xz} combined with the direct interlayer hopping of the d_2 orbital (dashed arrows in Fig. 1(a)). This mechanism generates the form

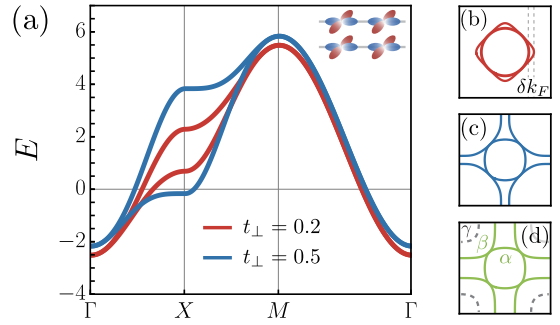


FIG. 2. (a) Band dispersion of the effective one-orbital model in Eq. 1. We set $t = 1$ and choose $t_{\perp} = 0.2$ and $t_{\perp} = 0.5$. The chemical potential is set to $\mu = -1.487$ and $\mu = -1.833$, respectively, to fix the average electron density of the d_1 orbital to $n_1 = 1 - x$ with $x = 0.5$. (b,c) Fermi surfaces for $t_{\perp} = 0.2$ (red) and $t_{\perp} = 0.5$ (blue). The interlayer hopping t_{\perp} splits the two bands and induces a Lifshitz transition. For small t_{\perp} , two electron pockets appear near Γ , while increasing t_{\perp} drives one of the electron pockets into a hole pocket at M . (d) For comparison, we show the Fermi surface of the two-orbital model in Eq. S1, hosting the α , β , and γ pockets.

factor $(\cos k_x - \cos k_y)^2$ in $\gamma(\mathbf{k})$. For simplicity, we drop the subscript x and use the notation $t = t_x$ and $t_{\perp} = t_x^{\perp}$, and throughout this paper we set $t = 1$. The chemical potential μ is chosen to fix the electron density of the d_1 orbital to $n_1 = 1 - x$, where x denotes the hole doping. We mainly focus on $x = 0.5$, corresponding to the $d^{7.5}$ electron configuration of the material. In Fig. 2, we plot the band dispersion of Eq. (1) for two representative values, $t_{\perp} = 0.2$ and 0.5 . For sufficiently large t_{\perp} , the interlayer hybridization induces a band splitting along the Γ - X - M line, resulting in an electron pocket near $\Gamma = (0, 0)$ and a hole pocket near $M = (\pi, \pi)$. These features reproduce the α and β pockets of the original two-orbital model.

We further introduce an external electric displacement field that breaks mirror symmetry between the two layers, which is the central tuning parameter of our study. The resulting total noninteracting Hamiltonian becomes

$$H_{\text{eff}} = H_0^{\text{eff}} + D \sum_k (n_{t,k} - n_{b,k}), \quad (4)$$

where D denotes the strength of the displacement field. In the following, we will use this effective model to analyze superconducting instabilities.

Mean-field theory.— We now turn to interaction effects. We consider a phenomenological attractive interaction between the two layers, analogous to the effective interaction in conventional Bardeen–Cooper–Schrieffer (BCS) theory. Specifically, we assume an interlayer interaction of the form,

$$H_{\text{int}} = \frac{J_{\perp}^{\text{eff}}}{2} \sum_i \left[\mathbf{S}_{t,i} \cdot \mathbf{S}_{b,i} - \frac{1}{4} n_{t,i} n_{b,i} \right]. \quad (5)$$

While our aim is to demonstrate the qualitative possibility of a PDW state, a more quantitative description would require a strong-coupling approach based on detailed microscopic models, which we leave for future work. We emphasize that J_{\perp}^{eff} here is not simply the J_{\perp} of the d_{z^2} orbital; rather, it is treated as an effective attraction. A more rigorous analysis would need to incorporate the local moments from the d_{z^2} orbital and interlayer repulsion [75]. Since we expect our qualitative results to depend primarily on the pairing symmetry, we employ this simplified model for illustrative purposes.

We perform a standard mean-field analysis using an ansatz for the interlayer pairing order parameter,

$$\langle c_{t,i\uparrow} c_{b,i\downarrow} \rangle = \Delta_{\mathbf{Q}} \exp(i\mathbf{R}_i \cdot \mathbf{Q}), \quad (6)$$

where \mathbf{Q} denotes the center-of-mass momentum of the Cooper pair. The resulting mean-field Hamiltonian is given by,

$$H_{\text{MF}} = H_{\text{eff}} - \frac{J_{\perp}^{\text{eff}}}{2} \sum_{\mathbf{k}} \Delta_{\mathbf{Q}} c_{t,\mathbf{k}^+}^{\dagger} (i\sigma_y) c_{b,-\mathbf{k}^-}^{\dagger} + \text{H.c.}, \quad (7)$$

where $\mathbf{k}^{\pm} = \mathbf{k} \pm \mathbf{Q}/2$, such that $(\mathbf{k}^+, -\mathbf{k}^-)$ forms a Cooper pair carrying a total momentum \mathbf{Q} . The chemical potential μ is adjusted to fix the total electron density at $n = 1 - x$. For each \mathbf{Q} , the pairing amplitude $\Delta_{\mathbf{Q}}$ is determined self-consistently from H_{MF} . To identify the stable phase, we compute the mean-field free energy and compare it across different values of \mathbf{Q} . Since the system lacks perfect nesting and the Fermi-momentum mismatch $|k_{F,+} - k_{F,-}|$ is not uniquely defined, we perform our analysis with $\mathbf{Q} = (Q, 0)$ along the x -direction, scanning all possible $Q \in [0, \pi]$. This mean-field approach allows us to determine the energetically favored state as a function of the system parameters.

Pair-density-wave.— Our mean-field analysis reveals that breaking mirror symmetry via an external electric displacement field stabilizes a PDW state, similar to the Fulde–Ferrell (FF) phase. The primary results are summarized in Fig. 3.

Fig. 3(a) presents the zero-temperature phase diagram in the (D, t_{\perp}) plane at $x = 0.5$, which corresponds to the $d^{7.5}$ electron configuration. Three distinct phases are identified: (I) a uniform superconducting (SC) phase where $\Delta_0 \neq 0$, (II) a pair-density-wave (PDW) phase characterized by $\Delta_{\mathbf{Q}} \neq 0$ with $\mathbf{Q} \neq 0$, and (III) a normal metallic phase with $\Delta_0 = \Delta_{\mathbf{Q}} = 0$ for all \mathbf{Q} . For a fixed t_{\perp} , increasing the displacement field D drives a transition from the uniform SC phase to the PDW phase, with the PDW phase appearing in the intermediate regime. At sufficiently large D , strong mirror-symmetry breaking induces a significant energy splitting between the layers, which suppresses interlayer pairing and stabilizes a normal metallic state, even at zero temperature.

Increasing t_{\perp} tends to destabilize the PDW phase; in the large- t_{\perp} limit, the system favors a uniform s^{\pm} pairing state instead. Fig. 3(b) shows the optimal ordering

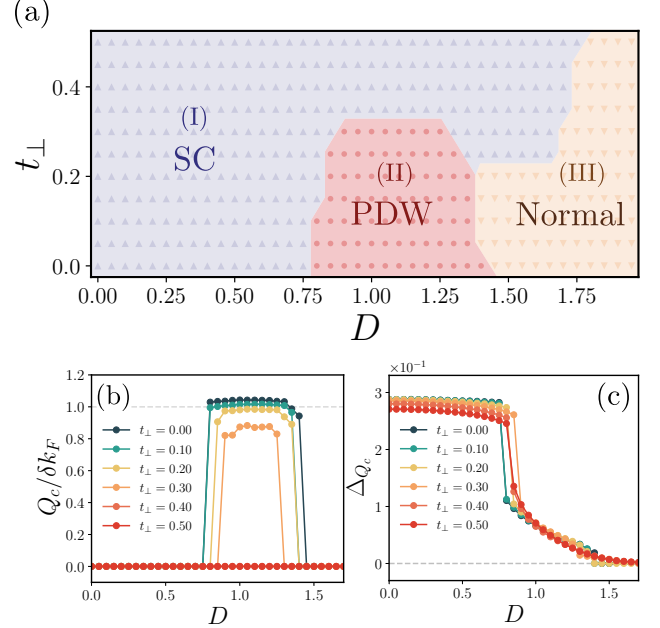


FIG. 3. (a) Zero-temperature mean-field phase diagram in the (D, t_{\perp}) plane. We fix $J_{\perp} = 4$ and $x = 1/2$. As D increases, the system undergoes consecutive transitions from a uniform superconducting (SC) phase to a pair-density-wave (PDW) phase, and finally to a normal state. (b, c) Mean-field solutions that minimize the free energy. For small t_{\perp} , the optimal pairing momentum Q is close to δk_F , the Fermi-momentum difference along the x -direction as illustrated in Fig. 2(b), while it deviates from this value as t_{\perp} increases. The transition between the uniform SC and PDW phases is of first order.

wave vector \mathbf{Q}_c . For small t_{\perp} , \mathbf{Q}_c is close to δk_F , but it deviates as t_{\perp} increases. This deviation occurs because δk_F is defined in the bonding–antibonding band basis, $\delta k_F = k_{F,+} - k_{F,-}$, whereas the pairing occurs between electrons on different layers in the real-space basis.

Fig. 3(c) demonstrates that the transition between the uniform SC and PDW phases is first-order, while the transitions between the PDW and normal phases, or between the SC and normal phases, are continuous. Although the form factor in the interlayer hopping t_{\perp} is motivated by the specific band structure of bilayer nickelates, we find that it does not qualitatively alter the phase diagram and PDW is more stabilized in case of without form factor, due to better nesting condition (See Fig. S1). Consequently, similar PDW phases could be realized more generally in other bilayer systems subject to an external electric field. Finally, Fig. 4 examines the dependence on electron filling, demonstrating that the PDW phase remains robust against doping.

Generalized Anderson theorem.— We have shown that a mirror-symmetry breaking term, such as the displacement field D , significantly alters the phase diagram. We now turn our attention to disorder that breaks mirror re-

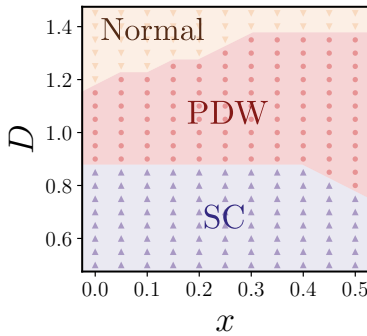


FIG. 4. Filling dependence of the zero-temperature mean-field phase diagram, where we fix $t_{\perp} = 0.1$ and $J_{\perp} = 4$. The PDW phase appears over a wide range of filling x .

flection symmetry only locally. For conventional s -wave superconductors, Anderson's theorem states that the pairing is stable against disorder as long as time-reversal symmetry \mathcal{T} remains unbroken. For our interlayer-paired superconductor, however, we demonstrate that disorder breaking mirror symmetry can suppress pairing even when time-reversal symmetry is preserved.

We consider a general spin-independent disorder potential defined in the two-layer basis,

$$V_{\text{dis}} = \sum_{i=0,1,2,3} V_i \tau_i \otimes \sigma_0, \quad (8)$$

where τ_i and σ_i are Pauli matrices acting in layer and spin space, respectively. The symmetry properties of the disorder channels are determined by the antiunitary time-reversal operator $\mathcal{T} = i\sigma_y K$, where K denotes complex conjugation, and the unitary mirror-reflection operator $\mathcal{M} = \tau_x$. Accordingly, the four disorder channels are classified as, (i) mirror-symmetric and time-reversal-symmetric (V_0), (ii) mirror-symmetric and interlayer time-reversal-symmetric (V_1), (iii) mirror-antisymmetric and time-reversal-antisymmetric (V_2), and (iv) mirror-antisymmetric and time-reversal-symmetric (V_3).

We treat disorder perturbatively within the first-order Born approximation. We first consider the case $t_{\perp} = 0$, for which the two bands are degenerate. In this limit, following Ref. [116], the disorder-induced suppression of the critical temperature T_c can be expressed in terms of the superconducting fitness function F_c [117],

$$\log \left(\frac{T_c}{T_{c,0}} \right) = -\frac{\pi}{4} \frac{\alpha_{\text{dis}}}{T_{c,0}} \Gamma, \quad (9)$$

where T_c is linearly suppressed by the effective scattering frequency, $\Gamma \equiv \pi N(0) n_{\text{imp}} V^2$ is used. $T_{c,0}$ denotes the critical temperature in the absence of disorder and $N(0)$ is the density of states at the Fermi energy. The dimensionless depairing coefficient α_{dis} is given by,

$$\alpha_{\text{dis}} = \frac{1}{4} \text{Tr} \left(\tilde{F}_c^{\dagger} \tilde{F}_c \right), \quad (10)$$

Disorder	\mathcal{M}	\mathcal{T}	Stab. of Δ_{\perp}
V_0	+	+	✓
V_1	+	+	✓
V_2	-	-	✓
V_3	-	+	✗

TABLE I. Summary of the generalized Anderson theorem for interlayer spin-singlet pairing, $\Delta_{\perp} = \tau_x \otimes i\sigma_y$. The second and third columns list the symmetry properties under mirror reflection \mathcal{M} and time-reversal symmetry \mathcal{T} for the four disorder potentials. The fourth column indicate the stability of interlayer pairing for both cases without ($t_{\perp} = 0$) and with ($t_{\perp} \neq 0$) interlayer hopping, determined by the depairing coefficient α_{dis} . A \checkmark denotes $\alpha_{\text{dis}} = 0$ (stable SC), while a \times denotes $\alpha_{\text{dis}} \neq 0$ (fragile SC).

with the fitness function defined as,

$$\tilde{F}_c = \hat{V}_{\text{dis}} \hat{\Delta} - \hat{\Delta} \hat{V}_{\text{dis}}^*. \quad (11)$$

It is important to note that \hat{V}_{dis} , $\hat{\Delta}$ denotes normalized quantity divided by the disorder strength and the superconducting gap. The depairing coefficient α_{dis} quantifies the robustness of the superconducting state, where a larger α_{dis} corresponds to a more fragile state, while $\alpha_{\text{dis}} = 0$ indicates complete robustness in the weak-disorder limit.

For $t_{\perp} = 0$ and interlayer spin-singlet pairing, $\Delta_{\perp} = \tau_x \otimes i\sigma_y$, we derive that $F_c = 0$ when the disorder potential possesses \mathcal{MT} symmetry. This implies that interlayer spin-singlet superconductivity is stable under \mathcal{MT} -preserving disorder scattering. Accordingly, Anderson's theorem for interlayer pairing should be modified to require \mathcal{MT} symmetry preservation. Applying the same analysis to intralayer pairing, $\Delta_{\parallel} = \tau_0 \otimes i\sigma_y$, we recover the conventional Anderson theorem, where the non-pair-breaking condition is simply the preservation of \mathcal{T} . The results are summarized in Table I.

Another important question is how this generalized Anderson theorem is modified in the presence of finite interlayer hopping t_{\perp} . To address this, we extend our analysis of α_{dis} to the $t_{\perp} \neq 0$ case. Our derivation reveals that the expression for α_{dis} (Eq. 10) remains invariant even under the band splitting induced by t_{\perp} . Hence underlying symmetry plays a more important role in determining robustness under weak disorder than the specific microscopic details of the Hamiltonian.

Consequently, the generalized Anderson theorem established here remains applicable in realistic experimental settings where disorder is typically time-reversal symmetric. Notably, for mirror-symmetry-breaking disorder (V_3), α_{dis} remains non-zero for both $t_{\perp} = 0$ and $t_{\perp} \neq 0$, even though the clean-limit critical temperature $T_{c,0}$ is rescaled by the modified density of states (DOS). In real materials, individual defects are likely to break mirror symmetry locally. Therefore, T_c in bilayer nickelates is expected to be sensitive to disorder, and higher T_c values

can be achieved in cleaner samples.

Conclusion.— In this work, we have shown that breaking mirror symmetry via a displacement field in bilayer nickelates provides a natural tuning knob for realizing a pair-density-wave (PDW) state. Within a mean-field framework, we demonstrated that the PDW phase is robust over a wide region of the parameter space. Furthermore, through an analysis of disorder effects using the superconducting fitness formalism, we generalized Anderson's theorem to interlayer spin-singlet pairing, showing that mirror-breaking disorder suppresses superconductivity. Our results establish bilayer nickelates as a tunable platform for engineering finite-momentum superconductivity and exploring symmetry-protected robustness against disorder.

Note added.— During the finalization of this manuscript, we became aware of a preprint [78], which also investigated a possible Fulde–Ferrell (FF) state driven by a displacement field.

Acknowledgements.— H.O. and Y.-H.Z. are supported by a startup fund from Johns Hopkins University and the Alfred P. Sloan Foundation through a Sloan Research Fellowship (Y.-H.Z.).

* Corresponding author: hoh22@jh.edu

- [1] H. Sun, M. Huo, X. Hu, J. Li, Z. Liu, Y. Han, L. Tang, Z. Mao, P. Yang, B. Wang, *et al.*, Signatures of superconductivity near 80 k in a nickelate under high pressure, *Nature* **621**, 493 (2023).
- [2] J. Hou, P.-T. Yang, Z.-Y. Liu, J.-Y. Li, P.-F. Shan, L. Ma, G. Wang, N.-N. Wang, H.-Z. Guo, J.-P. Sun, Y. Uwatoko, M. Wang, G.-M. Zhang, B.-S. Wang, and J.-G. Cheng, Emergence of High-Temperature Superconducting Phase in Pressurized $\text{La}_3\text{Ni}_2\text{O}_7$ Crystals, *Chinese Physics Letters* **40**, 117302 (2023).
- [3] G. Wang, N. N. Wang, X. L. Shen, J. Hou, L. Ma, L. F. Shi, Z. A. Ren, Y. D. Gu, H. M. Ma, P. T. Yang, Z. Y. Liu, H. Z. Guo, J. P. Sun, G. M. Zhang, S. Calder, J.-Q. Yan, B. S. Wang, Y. Uwatoko, and J.-G. Cheng, Pressure-Induced Superconductivity In Polycrystalline $\text{La}_3\text{Ni}_2\text{O}_{7-\delta}$, *Phys. Rev. X* **14**, 011040 (2024).
- [4] Y. Zhang, D. Su, Y. Huang, Z. Shan, H. Sun, M. Huo, K. Ye, J. Zhang, Z. Yang, Y. Xu, Y. Su, R. Li, M. Smidman, M. Wang, L. Jiao, and H. Yuan, High-temperature superconductivity with zero resistance and strange-metal behaviour in $\text{La}_3\text{Ni}_2\text{O}_{7-\delta}$, *Nature Physics* **20**, 1269 (2024).
- [5] H. Oh and Y.-H. Zhang, Type-II $t-J$ model and shared superexchange coupling from hund's rule in superconducting $\text{La}_3\text{Ni}_2\text{O}_7$, *Phys. Rev. B* **108**, 174511 (2023).
- [6] C. Lu, Z. Pan, F. Yang, and C. Wu, Interlayer coupling driven high-temperature superconductivity in $\text{La}_3\text{Ni}_2\text{O}_7$ under pressure (2023), [arXiv:2307.14965 \[cond-mat.supr-con\]](https://arxiv.org/abs/2307.14965).
- [7] H. Yang, H. Oh, and Y.-H. Zhang, Strong pairing from a small fermi surface beyond weak coupling: Application to $\text{La}_3\text{Ni}_2\text{O}_7$, *Phys. Rev. B* **110**, 104517 (2024).
- [8] X.-Z. Qu, D.-W. Qu, J. Chen, C. Wu, F. Yang, W. Li, and G. Su, Bilayer $t-J-J_{\perp}$ model and magnetically mediated pairing in the pressurized nickelate $\text{La}_3\text{Ni}_2\text{O}_7$, *Phys. Rev. Lett.* **132**, 036502 (2024).
- [9] H. Lange, L. Homeier, E. Demler, U. Schollwöck, A. Bohrdt, and F. Grusdt, Pairing dome from an emergent feshbach resonance in a strongly repulsive bilayer model (2023), [arXiv:2309.13040 \[cond-mat.str-el\]](https://arxiv.org/abs/2309.13040).
- [10] H. Lange, L. Homeier, E. Demler, U. Schollwöck, F. Grusdt, and A. Bohrdt, Feshbach resonance in a strongly repulsive ladder of mixed dimensionality: A possible scenario for bilayer nickelate superconductors, *Phys. Rev. B* **109**, 045127 (2024).
- [11] D.-C. Lu, M. Li, Z.-Y. Zeng, W. Hou, J. Wang, F. Yang, and Y.-Z. You, Superconductivity from doping symmetric mass generation insulators: Application to $\text{La}_3\text{Ni}_2\text{O}_7$ under pressure, arXiv preprint [arXiv:2308.11195](https://arxiv.org/abs/2308.11195) (2023).
- [12] G. Duan, Z. Liao, L. Chen, Y. Wang, R. Yu, and Q. Si, Orbital-selective correlation effects and superconducting pairing symmetry in a multiorbital $t-j$ model for bilayer nickelates, arXiv preprint [arXiv:2502.09195](https://arxiv.org/abs/2502.09195) (2025).
- [13] J.-X. Zhang, H.-K. Zhang, Y.-Z. You, and Z.-Y. Weng, Strong pairing originated from an emergent \mathbb{Z}_2 berry phase in $\text{La}_3\text{Ni}_2\text{O}_7$, arXiv preprint [arXiv:2309.05726](https://arxiv.org/abs/2309.05726) (2023).
- [14] Z. Luo, X. Hu, M. Wang, W. Wú, and D.-X. Yao, Bilayer two-orbital model of $\text{La}_3\text{Ni}_2\text{O}_7$ under pressure, *Phys. Rev. Lett.* **131**, 126001 (2023).
- [15] Y. Zhang, L.-F. Lin, A. Moreo, and E. Dagotto, Electronic structure, orbital-selective behavior, and magnetic tendencies in the bilayer nickelate superconductor $\text{La}_3\text{Ni}_2\text{O}_7$ under pressure, arXiv preprint [arXiv:2306.03231](https://arxiv.org/abs/2306.03231) (2023).
- [16] J. Huang, Z. Wang, and T. Zhou, Impurity and vortex states in the bilayer high-temperature superconductor $\text{La}_3\text{Ni}_2\text{O}_7$, *Physical Review B* **108**, 174501 (2023).
- [17] Y. Zhang, L.-F. Lin, A. Moreo, T. A. Maier, and E. Dagotto, Structural phase transition, $s\pm$ -wave pairing, and magnetic stripe order in bilayered superconductor $\text{La}_3\text{Ni}_2\text{O}_7$ under pressure, *Nature Communications* **15**, 2470 (2024).
- [18] B. Geisler, J. J. Hamlin, G. R. Stewart, R. G. Henning, and P. J. Hirschfeld, Structural transitions, octahedral rotations, and electronic properties of $\text{a}_3\text{ni}_2\text{o}_7$ rare-earth nickelates under high pressure, *npj Quantum Materials* **9**, 38 (2024).
- [19] L. C. Rhodes and P. Wahl, Structural routes to stabilize superconducting $\text{La}_3\text{Ni}_2\text{O}_7$ at ambient pressure, *Phys. Rev. Mater.* **8**, 044801 (2024).
- [20] Y. Zhang, L.-F. Lin, A. Moreo, T. A. Maier, and E. Dagotto, Electronic structure, magnetic correlations, and superconducting pairing in the reduced ruddlesden-popper bilayer $\text{La}_3\text{Ni}_2\text{O}_6$ under pressure: Different role of $d_{3z^2-r^2}$ orbital compared with $\text{La}_3\text{Ni}_2\text{O}_7$, *Phys. Rev. B* **109**, 045151 (2024).
- [21] H. Sakakibara, N. Kitamine, M. Ochi, and K. Kuroki, Possible high T_c superconductivity in $\text{La}_3\text{Ni}_2\text{O}_7$ under high pressure through manifestation of a nearly half-filled bilayer hubbard model, *Phys. Rev. Lett.* **132**, 106002 (2024).
- [22] Y.-H. Tian, Y. Chen, J.-M. Wang, R.-Q. He, and Z.-Y. Lu, Correlation effects and concomitant two-orbital

$s\pm$ -wave superconductivity in $La_3Ni_2O_7$ under high pressure, *Physical Review B* **109**, 165154 (2024).

[23] Q. Qin and Y.-f. Yang, High- t_c superconductivity by mobilizing local spin singlets and possible route to higher t_c in pressurized $La_3Ni_2O_7$, arXiv preprint arXiv:2308.09044 (2023).

[24] Y.-f. Yang, G.-M. Zhang, and F.-C. Zhang, Minimal effective model and possible high- t_c mechanism for superconductivity of $La_3Ni_2O_7$ under high pressure, arXiv preprint arXiv:2308.01176 (2023).

[25] J. Zhan, Y. Gu, X. Wu, and J. Hu, Cooperation between electron-phonon coupling and electronic interaction in bilayer nickelates $La_3Ni_2O_7$ (2024), [arXiv:2404.03638 \[cond-mat.supr-con\]](https://arxiv.org/abs/2404.03638).

[26] Y. Chen, Y.-H. Tian, J.-M. Wang, R.-Q. He, and Z.-Y. Lu, Non-fermi liquid and antiferromagnetic correlations with hole doping in the bilayer two-orbital hubbard model of $La_3Ni_2O_7$ at zero temperature, arXiv preprint arXiv:2407.13737 (2024).

[27] Q.-G. Yang, H.-Y. Liu, D. Wang, and Q.-H. Wang, Possible $s\pm$ -wave superconductivity in $La_3Ni_2O_7$, arXiv preprint arXiv:2306.03706 (2023).

[28] Y. Gu, C. Le, Z. Yang, X. Wu, and J. Hu, Effective model and pairing tendency in bilayer ni-based superconductor $La_3Ni_2O_7$, arXiv preprint arXiv:2306.07275 (2023).

[29] Y.-B. Liu, J.-W. Mei, F. Ye, W.-Q. Chen, and F. Yang, The $s\pm$ -wave pairing and the destructive role of apical-oxygen deficiencies in $La_3Ni_2O_7$ under pressure, arXiv preprint arXiv:2307.10144 (2023).

[30] Y. Shen, M. Qin, and G.-M. Zhang, Effective bi-layer model Hamiltonian and density-matrix renormalization group study for the high-T c superconductivity in $La_3Ni_2O_7$ under high pressure, *Chinese Physics Letters* **40**, 127401 (2023).

[31] G. Heier, K. Park, and S. Y. Savrasov, Competing d_{xy} and $s\pm$ pairing symmetries in superconducting $La_3Ni_2O_7$: LDA + FLEX calculations, *Phys. Rev. B* **109**, 104508 (2024).

[32] X. Sui, X. Han, H. Jin, X. Chen, L. Qiao, X. Shao, and B. Huang, Electronic properties of the bilayer nickelates $R_3Ni_2O_7$ with oxygen vacancies ($R = La$ or ce), *Phys. Rev. B* **109**, 205156 (2024).

[33] M. Kakoi, T. Kaneko, H. Sakakibara, M. Ochi, and K. Kuroki, Pair correlations of the hybridized orbitals in a ladder model for the bilayer nickelate $La_3Ni_2O_7$, *Phys. Rev. B* **109**, L201124 (2024).

[34] Quantum phase transition driven by competing intralayer and interlayer hopping of ni- $d_{3z^2-r^2}$ orbitals in bilayer nickelates arXiv preprint arXiv:2507.111692025.

[35] Z. Pan, C. Lu, F. Yang, and C. Wu, Effect of rare-earth element substitution in superconducting $r_3Ni_2O_7$ under pressure, arXiv preprint arXiv:2309.06173 (2023).

[36] Z. Fan, J.-F. Zhang, B. Zhan, D. Lv, X.-Y. Jiang, B. Normand, and T. Xiang, Superconductivity in nickelate and cuprate superconductors with strong bilayer coupling, *Phys. Rev. B* **110**, 024514 (2024).

[37] Y. Zhang, L.-F. Lin, A. Moreo, T. A. Maier, and E. Dagotto, Electronic structure, self-doping, and superconducting instability in the alternating single-layer trilayer stacking nickelates $La_3Ni_2O_7$, *Phys. Rev. B* **110**, L060510 (2024).

[38] Y.-f. Yang, Decomposition of multilayer superconductivity with interlayer pairing, *Phys. Rev. B* **110**, 104507 (2024).

[39] C. Lu, Z. Pan, F. Yang, and C. Wu, Interplay of two E_g orbitals in superconducting $La_3Ni_2O_7$ under pressure, *Phys. Rev. B* **110**, 094509 (2024).

[40] Z. Luo, B. Lv, M. Wang, W. Wu, and D.-X. Yao, High- t_c superconductivity in $La_3Ni_2O_7$ based on the bilayer two-orbital t-j model, *npj Quantum Materials* **9**, 61 (2024).

[41] T. Kaneko, H. Sakakibara, M. Ochi, and K. Kuroki, Pair correlations in the two-orbital hubbard ladder: Implications for superconductivity in the bilayer nickelate $La_3Ni_2O_7$, *Phys. Rev. B* **109**, 045154 (2024).

[42] S. Ryee, N. Witt, and T. O. Wehling, Quenched pair breaking by interlayer correlations as a key to superconductivity in $La_3Ni_2O_7$, *Phys. Rev. Lett.* **133**, 096002 (2024).

[43] Z. Ouyang, M. Gao, and Z.-Y. Lu, Absence of electron-phonon coupling superconductivity in the bilayer phase of $La_3Ni_2O_7$ under pressure, *npj Quantum Materials* **9**, 80 (2024).

[44] D. A. Shilenko and I. V. Leonov, Correlated electronic structure, orbital-selective behavior, and magnetic correlations in double-layer $La_3Ni_2O_7$ under pressure, *Phys. Rev. B* **108**, 125105 (2023).

[45] Y. Cao and Y.-f. Yang, Flat bands promoted by hund's rule coupling in the candidate double-layer high-temperature superconductor $La_3Ni_2O_7$ under high pressure, *Phys. Rev. B* **109**, L081105 (2024).

[46] Z. Liao, L. Chen, G. Duan, Y. Wang, C. Liu, R. Yu, and Q. Si, Electron correlations and superconductivity in $La_3Ni_2O_7$ under pressure tuning, *Phys. Rev. B* **108**, 214522 (2023).

[47] Y. Zhang, L.-F. Lin, A. Moreo, T. A. Maier, and E. Dagotto, Trends in electronic structures and $s\pm$ -wave pairing for the rare-earth series in bilayer nickelate superconductor $r_3Ni_2O_7$, *Phys. Rev. B* **108**, 165141 (2023).

[48] X. Chen, P. Jiang, J. Li, Z. Zhong, and Y. Lu, Charge and spin instabilities in superconducting $La_3Ni_2O_7$, *Phys. Rev. B* **111**, 014515 (2025).

[49] Z. Ouyang, J.-M. Wang, J.-X. Wang, R.-Q. He, L. Huang, and Z.-Y. Lu, Hund electronic correlation in $La_3Ni_2O_7$ under high pressure, *Phys. Rev. B* **109**, 115114 (2024).

[50] Y. Wang, K. Jiang, Z. Wang, F.-C. Zhang, and J. Hu, Electronic and magnetic structures of bilayer $La_3Ni_2O_7$ at ambient pressure, *Phys. Rev. B* **110**, 205122 (2024).

[51] S. Bötzsel, F. Lechermann, J. Gondolf, and I. M. Eremin, Theory of magnetic excitations in the multilayer nickelate superconductor $La_3Ni_2O_7$, *Phys. Rev. B* **109**, L180502 (2024).

[52] Y. Tian and Y. Chen, Spin density wave and superconductivity in the bilayer t-j model of $La_3Ni_2O_7$ under renormalized mean-field theory, *Physical Review B* **112**, 014520 (2025).

[53] Y.-B. Liu, H. Sun, M. Zhang, Q. Liu, W.-Q. Chen, and F. Yang, Origin of the diagonal double-stripe spin density wave and potential superconductivity in bulk $La_3Ni_2O_7$ at ambient pressure, *Phys. Rev. B* **112**, 014510 (2025).

[54] Z. Liao, Y. Wang, L. Chen, G. Duan, R. Yu, and Q. Si, Orbital-selective electron correlations in high- t_c bilayer nickelates: from a global phase diagram to implications for spectroscopy, arXiv preprint arXiv:2412.21019

(2024).

[55] R. Jiang, J. Hou, Z. Fan, Z.-J. Lang, and W. Ku, Pressure Driven Fractionalization of Ionic Spins Results in Cupratelike High- T_c Superconductivity in $\text{La}_3\text{Ni}_2\text{O}_7$, *Phys. Rev. Lett.* **132**, 126503 (2024).

[56] Y. Yin, J. Zhan, B. Liu, and X. Han, The s_{\pm} pairing symmetry in the pressured $\text{La}_3\text{Ni}_2\text{O}_7$ from electron-phonon coupling, arXiv preprint arXiv:2502.21016 (2025).

[57] W. Xi, S.-L. Yu, and J.-X. Li, Transition from s_{\pm} -wave to $d_{x^2-y^2}$ -wave superconductivity driven by interlayer interaction in the bilayer two-orbital model of $\text{La}_3\text{Ni}_2\text{O}_7$, *Phys. Rev. B* **111**, 104505 (2025).

[58] T. Kaneko, M. Kakoi, and K. Kuroki, t - j model for strongly correlated two-orbital systems: Application to bilayer nickelate superconductors, arXiv preprint arXiv:2504.10114 (2025).

[59] J.-H. Ji, C. Lu, Z.-Y. Shao, Z. Pan, F. Yang, and C. Wu, A strong-coupling-limit study on the pairing mechanism in the pressurized $\text{La}_3\text{Ni}_2\text{O}_7$, arXiv preprint arXiv:2504.12127 (2025).

[60] Y. Wang, Y. Zhang, and K. Jiang, Electronic structure and disorder effect of $\text{La}_3\text{Ni}_2\text{O}_7$ superconductor, *Chinese Physics B* **34**, 047105 (2025).

[61] M. E. Haque, R. Ali, M. Masum, J. Hassan, and S. Naqib, Dft exploration of pressure dependent physical properties of the recently discovered $\text{La}_3\text{Ni}_2\text{O}_7$ superconductor, arXiv preprint arXiv:2504.15853 (2025).

[62] L. Shi, Y. Luo, W. Wu, and Y. Zhang, Theoretical investigation of high- t_c superconductivity in sr-doped $\text{La}_3\text{Ni}_2\text{O}_7$ at ambient pressure, arXiv preprint arXiv:2503.13197 (2025).

[63] Y. Gao, Robust s_{\pm} -wave pairing in a bilayer two-orbital model of pressurized $\text{La}_3\text{Ni}_2\text{O}_7$ without the γ fermi surface, arXiv preprint arXiv:2502.19840 (2025).

[64] C. Le, J. Zhan, X. Wu, and J. Hu, Landscape of correlated orders in strained bilayer nickelate thin films, arXiv preprint arXiv:2501.14665 (2025).

[65] X. Hu, W. Qiu, C.-Q. Chen, Z. Luo, and D.-X. Yao, Electronic structures and multi-orbital models of $\text{La}_3\text{Ni}_2\text{O}_7$ thin films at ambient pressure, arXiv preprint arXiv:2503.17223 (2025).

[66] Z.-Y. Shao, J.-H. Ji, C. Wu, D.-X. Yao, and F. Yang, Possible high-temperature superconductivity driven by perpendicular electric field in the $\text{La}_3\text{Ni}_2\text{O}_7$ single-bilayer film at ambient pressure, arXiv preprint arXiv:2411.13554 (2024).

[67] J. Huang and T. Zhou, Effective perpendicular electric field as a probe for interlayer pairing in ambient-pressure superconducting $\text{La}_{2.85}\text{Pr}_{0.15}\text{Ni}_2\text{O}_7$ thin films, *Phys. Rev. B* **112**, 054506 (2025).

[68] K. Ushio, S. Kamiyama, Y. Hoshi, R. Mizuno, M. Ochi, K. Kuroki, and H. Sakakibara, Theoretical study on ambient pressure superconductivity in $\text{La}_3\text{Ni}_2\text{O}_7$ thin films: structural analysis, model construction, and robustness of s_{\pm} -wave pairing, arXiv preprint arXiv:2506.20497 (2025).

[69] W. Qiu, Z. Luo, X. Hu, and D.-X. Yao, Pairing symmetry and superconductivity in $\text{La}_3\text{Ni}_2\text{O}_7$ thin films, arXiv preprint arXiv:2506.20727 (2025).

[70] Y.-H. Cao, K.-Y. Jiang, H.-Y. Lu, D. Wang, and Q.-H. Wang, Strain-engineered electronic structure and superconductivity in $\text{La}_3\text{Ni}_2\text{O}_7$ thin films, arXiv preprint arXiv:2507.13694 (2025).

[71] Z.-Y. Shao, C. Lu, M. Liu, Y.-B. Liu, Z. Pan, C. Wu, and F. Yang, Pairing without γ pocket in the $\text{La}_3\text{Ni}_2\text{O}_7$ thin film, arXiv preprint arXiv:2507.20287 (2025).

[72] H. Oh, B. Zhou, and Y.-H. Zhang, Type-II t - J model in charge transfer regime in bilayer $\text{La}_3\text{Ni}_2\text{O}_7$ and trilayer $\text{La}_4\text{Ni}_3\text{O}_{10}$, *Phys. Rev. B* **111**, L020504 (2025).

[73] J.-R. Xue and F. Wang, Magnetism and superconductivity in the t - j model of $\text{La}_3\text{Ni}_2\text{O}_7$ under multiband gutzwiller approximation, *Chinese Physics Letters* **41**, 057403 (2024).

[74] H. Yang, H. Oh, and Y.-H. Zhang, Strong pairing and symmetric pseudogap metal in a double kondo lattice model: From a nickelate superconductor to a tetralayer optical lattice, *Phys. Rev. B* **111**, L241102 (2025).

[75] H. Oh, H. Yang, and Y.-H. Zhang, High-temperature superconductivity from kinetic energy (2024), arXiv:2411.07292 [cond-mat.str-el].

[76] H. Oh, H. Yang, and Y.-H. Zhang, Doping a spin-one mott insulator: possible application to bilayer nickelate (2025), arXiv:2509.02673 [cond-mat.str-el].

[77] H.-X. Wang, H. Oh, T. Helbig, B. Y. Wang, J. Li, Y. Yu, H. Y. Hwang, H.-C. Jiang, Y.-M. Wu, and S. Raghu, Origin of spin stripes in bilayer nickelate $\text{La}_3\text{Ni}_2\text{O}_7$ (2025), arXiv:2509.25344 [cond-mat.supr-con].

[78] Z.-D. Fan and A. Vishwanath, Minimal two band model and experimental proposals to distinguish pairing mechanisms of the high- t_c superconductor $\text{La}_3\text{Ni}_2\text{O}_7$ (2025), arXiv:2512.05956 [cond-mat.str-el].

[79] G. Wang, N. Wang, Y. Wang, L. Shi, X. Shen, J. Hou, H. Ma, P. Yang, Z. Liu, H. Zhang, *et al.*, Observation of high-temperature superconductivity in the high-pressure tetragonal phase of $\text{La}_2\text{Pr}_{n-1}\text{Ni}_n\text{O}_{3n+1}$, arXiv preprint arXiv:2311.08212 (2023).

[80] M. Zhang, C. Pei, Q. Wang, Y. Zhao, C. Li, W. Cao, S. Zhu, J. Wu, and Y. Qi, Effects of pressure and doping on Ruddlesden-Popper phases $\text{La}_{n+1}\text{Ni}_n\text{O}_{3n+1}$, *Journal of Materials Science & Technology* **185**, 147 (2024).

[81] Y. Zhou, J. Guo, S. Cai, H. Sun, P. Wang, J. Zhao, J. Han, X. Chen, Y. Chen, Q. Wu, Y. Ding, T. Xiang, H. kwang Mao, and L. Sun, Investigations of key issues on the reproducibility of high- t_c superconductivity emerging from compressed $\text{La}_3\text{Ni}_2\text{O}_7$ (2024), arXiv:2311.12361 [cond-mat.supr-con].

[82] L. Wang, Y. Li, S.-Y. Xie, F. Liu, H. Sun, C. Huang, Y. Gao, T. Nakagawa, B. Fu, B. Dong, Z. Cao, R. Yu, S. I. Kawaguchi, H. Kadobayashi, M. Wang, C. Jin, H.-k. Mao, and H. Liu, Structure responsible for the superconducting state in $\text{La}_3\text{Ni}_2\text{O}_7$ at high-pressure and low-temperature conditions, *Journal of the American Chemical Society* **146**, 7506 (2024).

[83] J. Li, D. Peng, P. Ma, H. Zhang, Z. Xing, X. Huang, C. Huang, M. Huo, D. Hu, Z. Dong, X. Chen, T. Xie, H. Dong, H. Sun, Q. Zeng, H.-k. Mao, and M. Wang, Identification of superconductivity in bilayer nickelate $\text{La}_3\text{Ni}_2\text{O}_7$ under high pressure up to 100 gpa, *National Science Review*, nwaf220 (2025), <https://academic.oup.com/nsr/advance-article-pdf/doi/10.1093/nsr/nwaf220/63400099/nwaf220.pdf>.

[84] P. Puphal, P. Reiss, N. Enderlein, Y.-M. Wu, G. Khalilullin, V. Sundaramurthy, T. Priessnitz, M. Knauth, A. Suthar, L. Richter, M. Isobe, P. A. van Aken, H. Takagi, B. Keimer, Y. E. Suyolcu, B. Wehinger, P. Hansmann, and M. Hepting, Unconventional crystal structure of the high-pressure superconductor $\text{La}_3\text{Ni}_2\text{O}_7$, *Phys.*

Rev. Lett. **133**, 146002 (2024).

[85] Z. Dong, M. Huo, J. Li, J. Li, P. Li, H. Sun, L. Gu, Y. Lu, M. Wang, Y. Wang, and Z. Chen, Visualization of oxygen vacancies and self-doped ligand holes in $\text{La}_3\text{Ni}_2\text{O}_7-\delta$, *Nature* **630**, 847 (2024).

[86] X. Chen, J. Choi, Z. Jiang, J. Mei, K. Jiang, J. Li, S. Agrestini, M. Garcia-Fernandez, H. Sun, X. Huang, D. Shen, M. Wang, J. Hu, Y. Lu, K.-J. Zhou, and D. Feng, Electronic and magnetic excitations in $\text{La}_3\text{Ni}_2\text{O}_7$, *Nature Communications* **15**, 9597 (2024).

[87] X. Chen, J. Zhang, A. S. Thind, S. Sharma, H. LaBolita, G. Peterson, H. Zheng, D. P. Phelan, A. S. Botana, R. F. Klie, and J. F. Mitchell, Polymorphism in the ruddlesden–popper nickelate $\text{la}_3\text{ni}_2\text{o}_7$: Discovery of a hidden phase with distinctive layer stacking, *Journal of the American Chemical Society* **146**, 3640 (2024).

[88] G. Wang, N. Wang, T. Lu, S. Calder, J. Yan, L. Shi, J. Hou, L. Ma, L. Zhang, J. Sun, B. Wang, S. Meng, M. Liu, and J. Cheng, Chemical versus physical pressure effects on the structure transition of bilayer nickelates, *npj Quantum Materials* **10**, 1 (2025).

[89] Y. Li, X. Du, Y. Cao, C. Pei, M. Zhang, W. Zhao, K. Zhai, R. Xu, Z. Liu, Z. Li, J. Zhao, G. Li, Y. Qi, H. Guo, Y. Chen, and L. Yang, Electronic correlation and pseudogap-like behavior of high-temperature superconductor $\text{la}_3\text{ni}_2\text{o}_7$, *Chinese Physics Letters* **41**, 087402 (2024).

[90] M. Li, Y. Wang, C. Pei, M. Zhang, N. Li, J. Guan, M. Amboage, N. Adama, Q. Kong, Y. Qi, *et al.*, Distinguishing electronic band structure of single-layer and bilayer ruddlesden–popper nickelates probed by in-situ high pressure x-ray absorption near-edge spectroscopy, arXiv preprint arXiv:2410.04230 (2024).

[91] X. Zhou, W. He, K. Ni, M. Huo, D. Hu, Y. Zhu, E. Zhang, Z. Jiang, S. Zhang, S. Su, *et al.*, Revealing nanoscale structural phase separation in $\text{la}_3\text{ni}_2\text{o}_7$ single crystal via scanning near-field optical microscopy, arXiv preprint arXiv:2410.06602 (2024).

[92] J. Yang, H. Sun, X. Hu, Y. Xie, T. Miao, H. Luo, H. Chen, B. Liang, W. Zhu, G. Qu, C.-Q. Chen, M. Huo, Y. Huang, S. Zhang, F. Zhang, F. Yang, Z. Wang, Q. Peng, H. Mao, G. Liu, Z. Xu, T. Qian, D.-X. Yao, M. Wang, L. Zhao, and X. J. Zhou, Orbital-dependent electron correlation in double-layer nickelate $\text{La}_3\text{Ni}_2\text{O}_7$, *Nature Communications* **15**, 4373 (2024).

[93] R. Khasanov, T. J. Hicken, D. J. Gawryluk, V. Sazzari, I. Plokhikh, L. P. Sorel, M. Bartkowiak, S. Bötzsel, F. Lechermann, I. M. Eremin, H. Luetkens, and Z. Guguchia, Pressure-enhanced splitting of density wave transitions in $\text{la}_3\text{ni}_2\text{o}_7-\delta$, *Nature Physics* **21**, 430 (2025).

[94] Z. Huo, Z. Luo, P. Zhang, A. Yang, Z. Liu, X. Tao, Z. Zhang, S. Guo, Q. Jiang, W. Chen, D.-X. Yao, D. Duan, and T. Cui, Modulation of the octahedral structure and potential superconductivity of $\text{la}_3\text{ni}_2\text{o}_7$ through strain engineering, *Science China Physics, Mechanics & Astronomy* **68**, 237411 (2025).

[95] P. Li, G. Zhou, W. Lv, Y. Li, C. Yue, H. Huang, L. Xu, J. Shen, Y. Miao, W. Song, Z. Nie, Y. Chen, H. Wang, W. Chen, Y. Huang, Z.-H. Chen, T. Qian, J. Lin, J. He, Y.-J. Sun, Z. Chen, and Q.-K. Xue, Angle-resolved photoemission spectroscopy of superconducting $(\text{La},\text{Pr})_3\text{ni}_2\text{o}_7/\text{srlaalo}_4$ heterostructures, *National Science Review* , nwaf205 (2025).

[96] C. Yue, J.-J. Miao, H. Huang, Y. Hua, P. Li, Y. Li, G. Zhou, W. Lv, Q. Yang, F. Yang, H. Sun, Y.-J. Sun, J. Lin, Q.-K. Xue, Z. Chen, and W.-Q. Chen, Correlated electronic structures and unconventional superconductivity in bilayer nickelate heterostructures, *National Science Review* , nwaf253 (2025).

[97] L. Bhatt, A. Y. Jiang, E. K. Ko, N. Schnitzer, G. A. Pan, D. F. Segedin, Y. Liu, Y. Yu, Y.-F. Zhao, E. A. Morales, *et al.*, Resolving structural origins for superconductivity in strain-engineered $\text{la}_3\text{ni}_2\text{o}_7$ thin films, arXiv preprint arXiv:2501.08204 (2025).

[98] B. Y. Wang, Y. Zhong, S. Abadi, Y. Liu, Y. Yu, X. Zhang, Y.-M. Wu, R. Wang, J. Li, Y. Tarn, *et al.*, Electronic structure of compressively strained thin film $\text{la}_2\text{prni}_2\text{o}_7$, arXiv preprint arXiv:2504.16372 (2025).

[99] W. Sun, Z. Jiang, B. Hao, S. Yan, H. Zhang, M. Wang, Y. Yang, H. Sun, Z. Liu, D. Ji, *et al.*, Observation of superconductivity-induced leading-edge gap in sr-doped $\text{la}_3\text{ni}_2\text{o}_7$ thin films, arXiv preprint arXiv:2507.07409 (2025).

[100] Q. Li, J. Sun, S. Boetzel, M. Ou, Z.-N. Xiang, F. Lechermann, B. Wang, Y. Wang, Y.-J. Zhang, J. Cheng, *et al.*, Enhanced superconductivity in the compressively strained bilayer nickelate thin films by pressure, arXiv preprint arXiv:2507.10399 (2025).

[101] B. Hao, M. Wang, W. Sun, Y. Yang, Z. Mao, S. Yan, H. Sun, H. Zhang, L. Han, Z. Gu, J. Zhou, D. Ji, and Y. Nie, Superconductivity in sr-doped $\text{la}_3\text{ni}_2\text{o}_7$ thin films, *Nature Materials* **10**, 01038 (2025).

[102] S. Fan, M. Ou, M. Scholten, Q. Li, Z. Shang, Y. Wang, J. Xu, H. Yang, I. M. Eremin, and H.-H. Wen, Superconducting gaps revealed by stm measurements on $\text{la}_2\text{prni}_2\text{o}_7$ thin films at ambient pressure, arXiv preprint arXiv:2506.01788 (2025).

[103] J. Shen, Y. Miao, Z. Ou, G. Zhou, Y. Chen, R. Luan, H. Sun, Z. Feng, X. Yong, P. Li, *et al.*, Anomalous energy gap in superconducting $\text{la}_{2.85}\text{pr}_{0.15}\text{ni}_2\text{o}_7/\text{srlaalo}_4$ heterostructures, arXiv preprint arXiv:2502.17831 (2025).

[104] M. Wang, B. Hao, W. Sun, S. Yan, S. Sun, H. Zhang, Z. Gu, and Y. Nie, Electron-hole crossover in $\text{la}_{3-x}\text{sr}_x\text{ni}_2\text{o}_7-\delta$ thin films, arXiv preprint arXiv:2508.15284 (2025).

[105] E. K. Ko, Y. Yu, Y. Liu, L. Bhatt, J. Li, V. Thampy, C.-T. Kuo, B. Y. Wang, Y. Lee, K. Lee, J.-S. Lee, B. H. Goodge, D. A. Muller, and H. Y. Hwang, Signatures of ambient pressure superconductivity in thin film $\text{La}_3\text{Ni}_2\text{O}_7$, *Nature* **638**, 935 (2025).

[106] G. Zhou, W. Lv, H. Wang, Z. Nie, Y. Chen, Y. Li, H. Huang, W.-Q. Chen, Y.-J. Sun, Q.-K. Xue, and Z. Chen, Ambient-pressure superconductivity onset above 40 K in $(\text{La},\text{Pr})_3\text{Ni}_2\text{O}_7$ films, *Nature* **640**, 641 (2025).

[107] Y. Liu, E. K. Ko, Y. Tarn, L. Bhatt, J. Li, V. Thampy, B. H. Goodge, D. A. Muller, S. Raghu, Y. Yu, and H. Y. Hwang, Superconductivity and normal-state transport in compressively strained $\text{la}_2\text{prni}_2\text{o}_7$ thin films, *Nature Materials* **24**, 1221 (2025).

[108] B. Hao, M. Wang, W. Sun, Y. Yang, Z. Mao, S. Yan, H. Sun, H. Zhang, L. Han, Z. Gu, J. Zhou, D. Ji, and Y. Nie, Superconductivity and phase diagram in Sr-doped $\text{La}_{3-x}\text{Sr}_x\text{Ni}_2\text{O}_7$ thin films (2025), arXiv:2505.12603 [cond-mat.supr-con].

[109] D. F. Agterberg, J. S. Davis, S. D. Edkins, E. Fradkin, D. J. Van Harlingen, S. A. Kivelson, P. A. Lee, L. Radzihovsky, J. M. Tranquada, and Y. Wang, The physics of pair-density waves: cuprate superconductors and beyond, *Annual Review of Condensed Matter Physics* **11**, 231 (2020).

[110] P. Fulde and R. A. Ferrell, Superconductivity in a strong spin-exchange field, *Physical Review* **135**, A550 (1964).

[111] A. I. Larkin, Nonuniform state of superconductor, *Zh. Eksp. Teor. Fiz.* **47**, 1136 (1964).

[112] P. W. Anderson, Theory of dirty superconductors, *J. Phys. Chem. Solids* **11**, 26 (1959).

[113] K. Michaeli and L. Fu, Spin-orbit locking as a protection mechanism of the odd-parity superconducting state against disorder, *Phys. Rev. Lett.* **109**, 187003 (2012).

[114] M. Hoyer, M. S. Scheurer, S. V. Syzranov, and J. Schmalian, Pair breaking due to orbital magnetism in iron-based superconductors, *Phys. Rev. B* **91**, 054501 (2015).

[115] J. F. Dodaro and S. A. Kivelson, Generalization of anderson's theorem for disordered superconductors, *Phys. Rev. B* **98**, 174503 (2018).

[116] L. Andersen, A. Ramires, Z. Wang, T. Lorenz, and Y. Ando, Generalized anderson's theorem for superconductors derived from topological insulators, *Sci. Adv.* **6**, eaay6502 (2020).

[117] A. Ramires, D. F. Agterberg, and M. Sigrist, Tailoring T_c by symmetry principles: The concept of superconducting fitness, *Phys. Rev. B* **98**, 024501 (2018).

[118] A. Abrikosov and L. Gor'Kov, On the problem of the knight shift in superconductors, *Soviet Physics JETP* **12**, 337 (1961).

[119] H. Bruus and K. Flensberg, *Many-body quantum theory in condensed matter physics: an introduction* (Oxford university press, 2004).

Supplemental Material for “Pair-density-wave superconductivity and Anderson’s theorem in bilayer nickelates”

Hanbit Oh^{1,*}, and Ya-Hui Zhang¹

¹ *William H. Miller III Department of Physics and Astronomy,
Johns Hopkins University, Baltimore, Maryland, 21218, USA*

CONTENTS

References	5
I. Two orbital model	1
II. Details on Mean-field theory	2
A. Mean-field phase diagram without form factor	2
III. Details on computing α_{dis}	3
A. Setup	3
B. 1st order Born approximation	3
C. $t_{\perp} = 0$ case	4
Renormalized gap equation and T_c	5
D. $t_{\perp} \neq 0$ case	6
Renormalized gap equation and T_c	7

I. Two orbital model

We start from a two-orbital tight-binding model on a bilayer square lattice, described by the following Hamiltonian:

$$\begin{aligned}
 H_0 = & -t_x \sum_{l,\sigma} \sum_{\langle i,j \rangle} \left(d_{1,i,l,\sigma}^\dagger d_{1,j,l,\sigma} + \text{H.c.} \right) \\
 & -t_z \sum_{l,\sigma} \sum_{\langle i,j \rangle} \left(d_{2,i,l,\sigma}^\dagger d_{2,j,l,\sigma} + \text{H.c.} \right) \\
 & -t_{xz} \sum_{l,\sigma} \sum_{\langle i,j \rangle} \left((-1)^{s_{ij}} d_{1,i,l,\sigma}^\dagger d_{2,j,l,\sigma} + \text{H.c.} \right) \\
 & -t_z^\perp \sum_{i,\sigma} \left(d_{2,i,t,\sigma}^\dagger d_{2,i,b,\sigma} + \text{H.c.} \right) + \Delta \sum_i (n_{i,1} - n_{i,2}).
 \end{aligned} \tag{S1}$$

Here, $l = t, b$ labels the layer index, and $\sigma = \uparrow, \downarrow$ denotes the spin. We denote d_1 and d_2 as the $d_{x^2-y^2}$ and d_{z^2} orbitals, respectively. Interlayer hopping is included only for the d_2 orbital, reflecting its strong out-of-plane character, while direct interlayer hybridization of the d_1 orbital is negligible. The hopping parameters are estimated from density functional theory as $t_x = 0.485$, $t_z = 0.110$, $t_{xz} = 0.239$, and $t_z^\perp = 0.635$ [14]. The parameter Δ represents the crystal-field splitting between the two orbitals. The factor $s_{ij} = 1$ (-1) for bonds along the x (y) direction. The corresponding bond-dependent sign factor $(-1)^{s_{ij}}$ encodes the symmetry of the $d_{x^2-y^2}-d_{z^2}$ hybridization on the square lattice. On average, the electron filling is $n = 2 - x$ per site (summed over spin), with $x \approx 0.5$ relevant to experiments, corresponding to orbital fillings $n_1 \approx 0.5$ and $n_2 \approx 1$. The resulting band structure hosts α , β , and γ Fermi pockets, as depicted in Fig. 2(d). Previous studies have shown that the α and β pockets exhibit mixed orbital character, while the γ pocket is predominantly from the d_2 orbital.

II. Details on Mean-field theory

We consider the effective one orbital model, introduced in Eq. 1,

$$H_{\text{eff}} = \sum_{\mathbf{k}, \sigma} \phi_{\mathbf{k}, \sigma}^\dagger \begin{pmatrix} \xi(\mathbf{k}) + D & \gamma(\mathbf{k}) \\ \gamma(\mathbf{k}) & \xi(\mathbf{k}) - D \end{pmatrix} \phi_{\mathbf{k}, \sigma} = \sum_{\mathbf{k}} \phi_{\mathbf{k}, \sigma}^\dagger \mathcal{H}_N(\mathbf{k}) \phi_{\mathbf{k}, \sigma} \quad (\text{S2})$$

with $\phi_{\mathbf{k}, \sigma}^T = (c_{t, \mathbf{k}, \sigma}, c_{b, \mathbf{k}, \sigma})$ and

$$\xi(\mathbf{k}) = -t(\cos k_x + \cos k_y) - \mu, \quad (\text{S3})$$

$$\gamma(\mathbf{k}) = -t_\perp(\cos k_x - \cos k_y)^2, \quad (\text{S4})$$

and D is displacement field strength. Note that we implicitly set μ to fix the electron density $n = 1 - x$.

We next incorporate the phenomenological attractive interaction as similar setup of BCS theory. Specifically interlayer density interaction $J_\perp > 0$ is considered,

$$H_{\text{int}} = \frac{J_\perp}{2} \sum_i \left[S_{t,i} \cdot S_{b,i} - \frac{1}{4} n_{t,i} n_{b,i} \right]. \quad (\text{S5})$$

We then employ a standard mean-field analysis with an ansatz for the interlayer pairing order parameter,

$$\langle c_{t,i\uparrow} c_{b,i\downarrow} \rangle = -\langle c_{t,i\downarrow} c_{b,i\uparrow} \rangle = \Delta_{\mathbf{Q}} \exp(i \mathbf{R}_i \cdot \mathbf{Q}), \quad (\text{S6})$$

where \mathbf{Q} denotes the center-of-mass momentum of the Cooper pair.

The mean-field Hamiltonian in Nambu basis $\Phi_{\mathbf{k}} = (\phi_{\mathbf{k}^+, \uparrow} \phi_{-\mathbf{k}^-, \downarrow}^*)$ is

$$H_{\text{MF}} = \frac{1}{2} \sum_{\mathbf{k} \in B.Z.} \Phi_{\mathbf{k}}^\dagger \mathcal{H}_{\text{BdG}}(\mathbf{k}) \Phi_{\mathbf{k}} + E_0$$

with

$$\mathcal{H}_{\text{BdG}} = \begin{pmatrix} \mathcal{H}_N(\mathbf{k}^+) & \mathcal{H}_{\text{pair}} \\ \mathcal{H}_{\text{pair}}^\dagger & -\mathcal{H}_N^T(-\mathbf{k}^-) \end{pmatrix}, \quad \mathcal{H}_{\text{pair}} = -J_\perp \Delta \begin{pmatrix} 0 & 1 \\ 1 & 0 \end{pmatrix}, \quad (\text{S7})$$

and constant energy term

$$E_0 = \frac{1}{2} \sum_{\mathbf{k} \in B.Z.} \text{Tr}(\mathcal{H}_N(-\mathbf{k}^-)) + N J_\perp |\Delta|^2. \quad (\text{S8})$$

Here, $\mathbf{k}^\pm = \mathbf{k} \pm \mathbf{Q}/2$ is used.

For each \mathbf{Q} , the pairing amplitude $\Delta_{\mathbf{Q}}$ is determined self-consistently from H_{MF} and Eq. S6. To further identify the phase among all \mathbf{Q} , we should compute the mean-field free-energy,

$$F_{\text{MF}} = -T \log \left(\text{Tr} \left(e^{-H_{\text{MF}}/T} \right) \right) + E_0, \quad (\text{S9})$$

and compare F for different \mathbf{Q} . The above mean-field analysis allows us to determine the energetically favored state as a function of system parameters.

A. Mean-field phase diagram without form factor

We also present the zero-temperature mean-field phase diagram without the momentum-dependent form factor, taking $\gamma(\mathbf{k}) = t_\perp$. The resulting phase diagram exhibits the same qualitative features as that obtained with the form factor shown in Fig. 3(a). As illustrated in Fig. S1, the results show that PDW is more stable than without form factor case. This is related to the shape of Fermi-surface, where the nesting vector is more well-defined in the absence of the form factor.

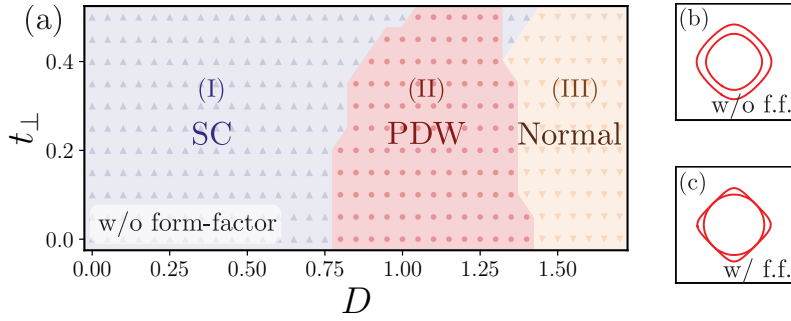


FIG. S1. (a) Zero-temperature mean-field phase diagram without a form factor, $t_{\perp}(\mathbf{k}) = t_{\perp}$. We fix $J_{\perp} = 4$ and $x = 1/2$. (b,c) Fermi surfaces without (b) and with (c) the form factor at $D = 0$. In the absence of the form factor, the nesting vector is relatively well defined, which stabilizes the PDW phase, compared to Fig. 3(a).

III. Details on computing α_{dis}

A. Setup

We again consider the two-band normal-state Hamiltonian,

$$H_N = \xi(\mathbf{k})\tau_0 + t_{\perp}(\mathbf{k})\tau_x, \quad (\text{S10})$$

where τ_i ($i = 0, 1, 2, 3$) are Pauli matrices defined in the layer basis. The corresponding band dispersions are given by $\xi_{\pm}(\mathbf{k}) = \xi(\mathbf{k}) \pm t_{\perp}(\mathbf{k})$, which become degenerate in the absence of interlayer hopping, $t_{\perp} = 0$.

Including interlayer pairing, the Bogoliubov–de Gennes (BdG) Hamiltonian can be written as

$$H_{\text{BdG}} = \begin{pmatrix} H_N(\mathbf{k}^+) & \Delta \\ \Delta^{\dagger} & -H_N^T(-\mathbf{k}^-) \end{pmatrix}, \quad (\text{S11})$$

with $\Delta = \Delta_0 \tau_1$.

We consider a general spin-independent disorder potential in the two-layer basis,

$$V_{\text{dis}} = \sum_{i=0,1,2,3} V_i \tau_i. \quad (\text{S12})$$

Here we restrict our analysis to the s -wave scattering channel, which is momentum independent.

It is convenient to transform from the layer basis to the band basis via a unitary transformation. Under this transformation, the Pauli matrices in the layer basis are mapped to those in the band basis as

$$\{\tau_0, \tau_1, \tau_2, \tau_3\} \rightarrow \{\tilde{\tau}_0, \tilde{\tau}_3, \tilde{\tau}_2, -\tilde{\tau}_1\}. \quad (\text{S13})$$

B. 1st order Born approximation

We then employ the conventional first-order Born approximation (1BA), treating V_{dis} as a perturbation [118, 119]. The corresponding self-energy is given by

$$\Sigma(i\omega_n) = n_{\text{imp}} \int_{\mathbf{k}} \tilde{V}_{\text{dis}} G_{\text{BdG}}(\mathbf{k}, i\omega_n) \tilde{V}_{\text{dis}}, \quad (\text{S14})$$

where $G_{\text{BdG}}(\mathbf{k}, i\omega_n) = (i\omega_n - H_{\text{BdG}})^{-1}$ is BdG Green's function and \tilde{V}_{dis} denotes the disorder potential written in the Nambu basis. $i\omega_n$ is the fermionic Matsubara frequency. A diagrammatic representation is shown in Fig. S1(a).

We then decompose the self-energy in Eq. S14 into contributions that renormalize the frequency and the pairing amplitude, denoted by Σ_{ω} and Σ_{Δ} , respectively. These are given by

$$\Sigma_{\omega}(\mathbf{k}, i\omega_n) = \lim_{\Delta_0 \rightarrow 0} \int_{\mathbf{k}} \frac{n_{\text{imp}} V^2}{2} \text{Tr} \left[\hat{V} G(\mathbf{k}, i\omega_n) \hat{V} \right], \quad (\text{S15})$$

and

$$\frac{\Sigma_\Delta(\mathbf{k}, i\omega_n)}{\Delta_0} = -\lim_{\Delta_0 \rightarrow 0} \int_{\mathbf{k}} \frac{n_{\text{imp}} V^2}{2\Delta_0} \text{Tr} \left[\hat{V} F(\mathbf{k}, i\omega_n) \hat{V}^* \hat{\Delta}^\dagger \right], \quad (\text{S16})$$

where G and F denote the diagonal and off-diagonal blocks of the BdG Green's function \mathcal{G}_{BdG} , respectively. The limit $\Delta_0 \rightarrow 0$ is taken since we will focus on the critical temperature, assuming that the superconducting transition is a continuous second-order phase transition. The hat notation in disorder potential and pairing denotes the normalized matrix, i.e. $\hat{\Delta} = \tau_1$.

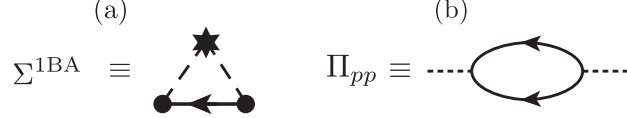


FIG. S2. Diagrammatic representation of (a) the first-order Born approximation and (b) the particle-particle susceptibility.

C. $t_\perp = 0$ case

We begin with the simple case $t_\perp = 0$, where the two bands are degenerate with dispersion $\xi_{\mathbf{k}}$. In the limit $\Delta_0 \rightarrow 0$, the normal and anomalous Green's functions simplify to

$$\lim_{\Delta_0 \rightarrow 0} G(\mathbf{k}, i\omega_n) = -\frac{i\omega_n + \xi_{\mathbf{k}}}{\omega_n^2 + \xi_{\mathbf{k}}^2}, \quad \lim_{\Delta_0 \rightarrow 0} \frac{F(\mathbf{k}, i\omega_n)}{\Delta_0} = -\frac{\hat{\Delta}}{\omega_n^2 + \xi_{\mathbf{k}}^2}. \quad (\text{S17})$$

Substituting these expressions into Eqs. S15 and S16, we obtain

$$\Sigma_\omega(\mathbf{k}, i\omega_n) = -\frac{i\omega_n}{|\omega_n|} \pi N(0) n_{\text{imp}} V^2, \quad (\text{S18})$$

and

$$\Sigma_\Delta(\mathbf{k}, i\omega_n) = \frac{\Delta_0}{|\omega_n|} \pi N(0) \frac{n_{\text{imp}} V^2}{2} \text{Tr} \left[\hat{V} \hat{\Delta} \hat{V}^* \hat{\Delta}^\dagger \right], \quad (\text{S19})$$

where we used $\int_{\mathbf{k}} = N(0) \int d\xi$, with $N(0)$ the density of states at the Fermi energy.

The trace part in Eq. S19 can be simplified using

$$\text{Tr} \left[\hat{V} \hat{\Delta} \hat{V}^* \hat{\Delta}^\dagger \right] = 2 - \frac{1}{2} \text{Tr} \left[\hat{F}_c^\dagger \hat{F}_c \right], \quad (\text{S20})$$

where the superconducting fitness function is defined as

$$F_c = V\Delta - \Delta V^*. \quad (\text{S21})$$

Substituting Eq. S20 into Eq. S19, we obtain

$$\Sigma_\Delta(\mathbf{k}, i\omega_n) = \frac{\Delta_0}{|\omega_n|} \pi N(0) n_{\text{imp}} V^2 \left[1 - \frac{1}{4} \text{Tr} \left(\hat{F}_c^\dagger \hat{F}_c \right) \right]. \quad (\text{S22})$$

The renormalized Matsubara frequency and pairing amplitude are therefore given by

$$\tilde{\omega}_n = \omega_n + \frac{\tilde{\omega}_n}{|\tilde{\omega}_n|} \Gamma, \quad (\text{S23})$$

$$\tilde{\Delta}_0 = \Delta_0 + \frac{\tilde{\Delta}_0}{|\tilde{\omega}_n|} \left[1 - \frac{1}{4} \text{Tr} \left(\tilde{F}_c^\dagger \tilde{F}_c \right) \right] \Gamma, \quad (\text{S24})$$

where scattering frequency, $\Gamma \equiv \pi N(0) n_{\text{imp}} V^2 = \tau^{-1}$ is used.

As we show in the next subsection, the ratio between $\tilde{\omega}_n/\tilde{\Delta}_0 \equiv u_n$ is central quantity in determining the disorder-induced suppression of the critical temperature, as obtained from the linearized gap equation. From Eqs. S23- S24, one can find

$$\frac{\omega_n}{\Delta_0} = u_n \left[1 - \frac{\alpha_{\text{dis}}}{\Delta_0} \frac{\Gamma}{|u_n|} \right] \quad (\text{S25})$$

with defining depairing coefficient

$$\alpha_{\text{dis}} = \frac{1}{4} \text{Tr}(\tilde{F}_c^\dagger \tilde{F}_c). \quad (\text{S26})$$

If the condition $\tilde{\omega}_n/\tilde{\Delta}_0 = \omega_n/\Delta_0$ is satisfied, meaning that the frequency and pairing renormalizations are identical (equivalently, $\alpha_{\text{dis}} = 0$), the superconducting state is robust against the corresponding disorder channel.

Finally, for the disorder channels $\hat{V} = \tau_i$ defined in Eq. S12 and interlayer pairing $\hat{\Delta} = \tau_1$, we find

$$F_c = 0, \quad \text{for all channels except } \tau_3. \quad (\text{S27})$$

consequently, $\alpha_{\text{dis}} = 0$ for all channels except τ_3 , while $\alpha_{\text{dis}} = 2$ for τ_3 . This result directly leads to Table I. The τ_3 disorder channel breaks the composite \mathcal{MT} symmetry, while all other channels preserve it.

Renormalized gap equation and T_c

We now evaluate the critical temperature in the presence (absence) of disorder, denoted by T_c ($T_{c,0}$). In the presence of impurity scattering, the gap equation is modified as

$$\frac{1}{2g} = \frac{T_{c,0}}{\mathcal{V}} \sum_{\mathbf{k}, \omega_n} \frac{1}{\omega_n^2 + \xi_{\mathbf{k}}^2} \rightarrow \frac{\Delta_0}{2g} = \frac{T_c}{\mathcal{V}} \sum_{\mathbf{k}, \omega_n} \frac{\tilde{\Delta}_0}{\tilde{\omega}_n^2 + \xi_{\mathbf{k}}^2}, \quad (\text{S28})$$

where $g > 0$ denotes the attractive pairing interaction. The gap equation is achieved by the second order Ginzburg Landau diagram as illustrated in Fig. S2(b).

Replacing the momentum summation by an integral over energies near the Fermi surface and using Eqs. S23-S24, the gap equation can be rewritten as

$$\frac{1}{2g} \simeq \pi N(0) T_{c,0} \sum_{|\omega_n| < \Lambda_{UV}} \frac{1}{|\omega_n|} \rightarrow \frac{\Delta_0}{2g} \simeq \pi N(0) T_c \sum_{|\omega_n| < \Lambda_{UV}} \frac{\tilde{\Delta}_0}{|\tilde{\omega}_n|}, \quad (\text{S29})$$

where Λ_{UV} is an ultraviolet energy cutoff imposed on the Matsubara frequencies.

Substituting the renormalized parameters from Eq. S25, we obtain

$$\frac{1}{2g} \simeq \pi N(0) T_c \sum_{|\omega_n| < \Lambda_{UV}} \left[\frac{1}{\omega_n} - \frac{\alpha_{\text{dis}}}{\omega_n^2} \Gamma \right] \quad (\text{S30})$$

To perform the Matsubara summation in Eq. S30, we make use of the digamma function $\Psi(z)$ and its derivative $\Psi^{(1)}(z) = d\Psi(z)/dz$ defined as

$$\Psi(z) = -\xi - \sum_{n=0}^{\infty} \left[\frac{1}{n+z} - \frac{1}{n+1} \right], \quad \Psi^{(1)}(z) = \sum_{n=0}^{\infty} \frac{1}{(n+z)^2},$$

where ξ denotes the Euler constant. For large $|z|$, the asymptotic forms $\Psi(z) \simeq \log z$ and $\Psi^{(1)}(z) \simeq 1/z$ can be used.

Applying these identities yields

$$\begin{aligned} 2\pi T_c \sum_{\omega_n=0}^{\Lambda_{UV}} \frac{1}{\omega_n} &= - \left[\Psi\left(\frac{1}{2}\right) - \Psi\left(\frac{1}{2} + \frac{\Lambda_{UV}}{2\pi T_c}\right) \right] \\ &\simeq - \left[\Psi\left(\frac{1}{2}\right) - \log\left(\frac{\Lambda_{UV}}{2\pi T_c}\right) \right], \end{aligned} \quad (\text{S31})$$

and

$$\begin{aligned} 2\pi T_c \sum_{\omega_n=0}^{\Lambda_{UV}} \frac{1}{\omega_n^2} &= \frac{1}{2\pi T_c} \left[\Psi^{(1)}\left(\frac{1}{2}\right) - \Psi^{(1)}\left(\frac{1}{2} + \frac{\Lambda_{UV}}{2\pi T_c}\right) \right] \\ &\simeq \frac{1}{2\pi T_c} \left[\frac{\pi^2}{2} - \frac{2\pi T_c}{\Lambda_{UV}} \right], \end{aligned} \quad (\text{S32})$$

valid in the limit $T_c \ll \Lambda_{UV}$.

Finally, we obtain the disorder-suppressed critical temperature,

$$\log\left(\frac{T_c}{T_{c,0}}\right) \simeq -\frac{\pi}{4} \frac{\alpha_{\text{dis}}}{T_{c,0}} \Gamma, \quad (\text{S33})$$

where the parameter α_{dis} quantifies the suppression of the critical temperature due to disorder.

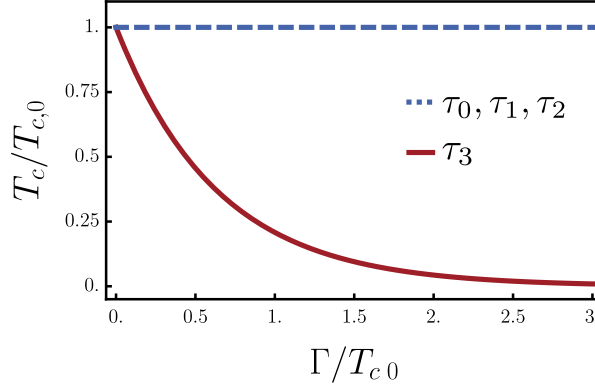


FIG. S3. Transition temperature T_c as a function of the scattering rate Γ , obtained from Eq. S43. The τ_3 disorder channel, which breaks mirror symmetry, suppresses superconductivity (i.e. $\alpha_{\text{dis}} = 2$) irrespective of whether $t_{\perp} = 0$ or finite.

D. $t_{\perp} \neq 0$ case

For the case where $t_{\perp} \neq 0$, the band splitting modifies the dispersion to $\xi_{\pm}(\mathbf{k}) = \xi(\mathbf{k}) \pm |t_{\perp}|$, which may modify the expression for the depairing coefficient α_{dis} . Following the framework introduced in Sec. III A, we evaluate the normal and anomalous Green's functions, G and F , in the limit $\Delta_0 \rightarrow 0$ to calculate the self-energies.

In the band basis, the normal Green's function is expressed as,

$$\begin{aligned} G_N(\mathbf{k}, i\omega_n) &= \frac{1}{2} \left[(i\omega_n - \xi_+(\mathbf{k}))^{-1} + (i\omega_n - \xi_-(\mathbf{k}))^{-1} \right] \tilde{\tau}_0 \\ &+ \frac{1}{2} \left[(i\omega_n - \xi_+(\mathbf{k}))^{-1} - (i\omega_n - \xi_-(\mathbf{k}))^{-1} \right] \tilde{\tau}_3, \end{aligned} \quad (\text{S34})$$

where the tilde notation denotes Pauli matrices defined in the band basis. The anomalous Green's function in the same limit is given by,

$$\lim_{\Delta_0 \rightarrow 0} \frac{F(\mathbf{k}, i\omega_n)}{\Delta_0} = G_N \hat{\Delta} G_N^* = G_N G_N^* \hat{\Delta}, \quad (\text{S35})$$

where we have used the fact that $[G_N, \hat{\Delta}] = 0$, as both operators are diagonal in the band basis (i.e., expressed in $\tilde{\tau}_0$ and $\tilde{\tau}_3$).

Substituting these expressions into the self-energy equations, we obtain the results for $t_{\perp} \neq 0$. For the frequency self-energy, we find,

$$\lim_{\Delta_0 \rightarrow 0} \text{Tr} \left[\hat{V} G(\mathbf{k}, i\omega_n) \hat{V} \right] = \text{Tr} \left[\left(G_N \hat{V} + [\hat{V}, G_N] \right) \hat{V} \right] = \text{Tr} \left[G_N \hat{V} \hat{V} \right] \quad (\text{S36})$$

$$= - \left(\frac{i\omega_n + \xi_+}{\omega_n^2 + \xi_+^2} + \frac{i\omega_n + \xi_-}{\omega_n^2 + \xi_-^2} \right), \quad (\text{S37})$$

and for the pairing self-energy,

$$\begin{aligned} \lim_{\Delta_0 \rightarrow 0} \frac{1}{\Delta_0} \text{Tr} \left[\hat{V} F(\mathbf{k}, i\omega_n) \hat{V}^* \hat{\Delta}^\dagger \right] &= \text{Tr} \left[([\hat{V}, G_N G_N^*] + G_N G_N^* \hat{V}) \hat{\Delta} \hat{V}^* \hat{\Delta}^\dagger \right] \\ &= \text{Tr} \left[G_N G_N^* \hat{V} \hat{\Delta} \hat{V}^* \hat{\Delta}^\dagger \right] \end{aligned} \quad (\text{S38})$$

$$= - \left(\frac{1}{\omega_n^2 + \xi_+^2} + \frac{1}{\omega_n^2 + \xi_-^2} \right) \times \left[1 - \frac{1}{4} \text{Tr}(\hat{F}_c^\dagger \hat{F}_c) \right]. \quad (\text{S39})$$

In Eqs. (S36) and (S38), the terms involving commutators vanish upon taking the trace $\text{Tr}([\hat{V}, G_N] \hat{V}) = \text{Tr}([\hat{V}, G_N G_N^*] \hat{\Delta} \hat{V}^* \hat{\Delta}^\dagger) = 0$, because \hat{V} is one of Pauli matrix $\tilde{\tau}_i$, and G_N and $G_N G_N^*$ are expressed only by $\{\tilde{\tau}_0, \tilde{\tau}_3\}$.

Performing the momentum summation, the effective density of states (DOS) is modified to $\bar{N}(0) = \frac{1}{2}(N_+(0) + N_-(0))$. Crucially, however, the ratio $u_n = \tilde{\omega}_n / \tilde{\Delta}_n$ remains identical to the $t_\perp = 0$ case (See Eq. S25),

$$u_n \equiv \frac{\omega_n}{\Delta_0} = u_n \left[1 - \frac{\alpha_{\text{dis}}}{\Delta_0} \frac{\Gamma}{|u_n|} \right], \quad (\text{S40})$$

with the same depairing coefficient,

$$\alpha_{\text{dis}} = \frac{1}{4} \text{Tr}(\tilde{F}_c^\dagger \tilde{F}_c). \quad (\text{S41})$$

Renormalized gap equation and T_c

We now evaluate the critical temperature in the presence of disorder, T_c . The linearized gap equation is given by,

$$\frac{1}{g} = \frac{T_c}{\mathcal{V}} \sum_{\mathbf{k}, \omega_n} \left[\frac{\tilde{\Delta}_0}{\tilde{\omega}_n^2 + \xi_{+, \mathbf{k}}^2} + \frac{\tilde{\Delta}_0}{\tilde{\omega}_n^2 + \xi_{-, \mathbf{k}}^2} \right]. \quad (\text{S42})$$

After performing the summation over momentum and Matsubara frequencies, we observe that since the ratio $u_n = \tilde{\omega}_n / \tilde{\Delta}_0$ is derived to be unchanged, the functional form of the T_c suppression remains the same with the $t_\perp = 0$ case,

$$\log \left(\frac{T_c}{T_{c,0}} \right) = - \frac{\pi}{4} \frac{\alpha_{\text{dis}}}{T_{c,0}} \Gamma. \quad (\text{S43})$$

While the same ratio between $T_c / T_{c,0}$ holds, the clean-limit critical temperature $T_{c,0}$ itself is rescaled by the change in the DOS,

$$\frac{T_{c,0}(t_\perp)}{T_{c,0}(t_\perp = 0)} = \frac{2N(0)}{N_+(0) + N_-(0)}, \quad (\text{S44})$$

where $N_\pm(0)$ denotes the DOS of the ξ_\pm band at the Fermi level.